Supplementary Information

Robust Superwetting Sintered Glass Filters for High-Pressure Separation of Emulsions with Enhanced Flux and High-Viscosity-Oil Tolerance

*Weishi Wang, Wenqing Cao, Yingqi Qiu, Yue Liu and Lin Feng**

1. Influence of the Thickness of the Substrate SGF on Its Pressure Resistance.

To simulate the structure of the high-pressure separation device designed in this work, we conducted pressure resistance tests on substrates with different thicknesses from an initial thickness of 2 mm to 5 mm (due to limitations of the substrate fabrication process, the minimum thickness gradient was 1 mm). Specifically, we simplified the pressure filtration structure: a circular ring with an outer diameter of 40 mm (consistent with the substrate SGF) and an inner hollow diameter of 35 mm was used as the base. After aligning the substrate with the base, a solid cylindrical iron block with a diameter of 30 mm was placed at the center of the substrate's upper surface. The entire assembly was then compressed at a speed of 10 mm/min to simulate the longitudinal pressure exerted on the material during high-pressure separation. As shown in the figure below, the stress of SGF grew significantly as the thickness increased, which fully demonstrated that the thickness of robust sintered glass filter improves its pressure resistance, and in future researches could be further enhanced by increasing the thickness as needed.

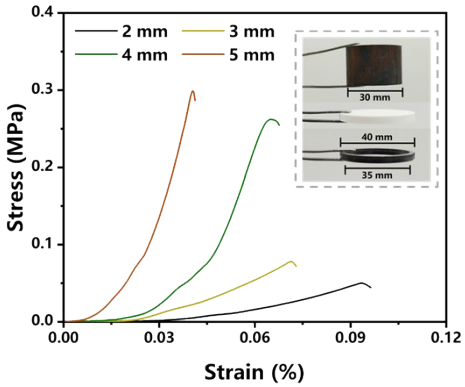

Fig. S1 Stress-strain curves of substrates (SGF) with different thicknesses.

2. Pore Size Changes of Sintered Glass Filter Before and After Polydopamine Modification.

The average pore sizes were calculated based on the 5000×SEM images of the material before and after polydopamine modification. As shown in the figure below, the average pore size was 1.47 μm before modification and 1.27 μm after modification, showing only a slight decrease. This confirms that polydopamine modification did not significantly reduce the pore size of the material.

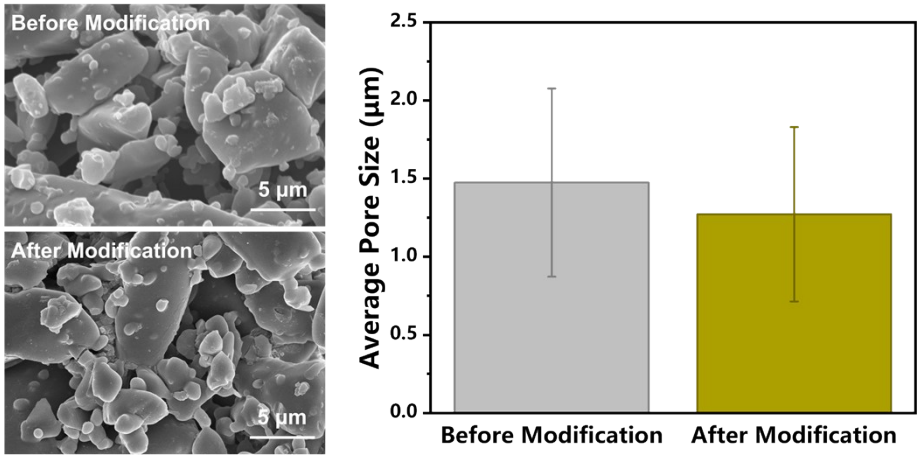

Fig. S2 SEM Images (5000×) and Pore Size Changes of the Material Before and After Polydopamine Modification.

3. Surface Element Distribution and Proportion of Substrate SGF and PDA-SGF.

Energy Dispersive X-ray Spectroscopy (EDX) elemental analysis was conducted on the samples.

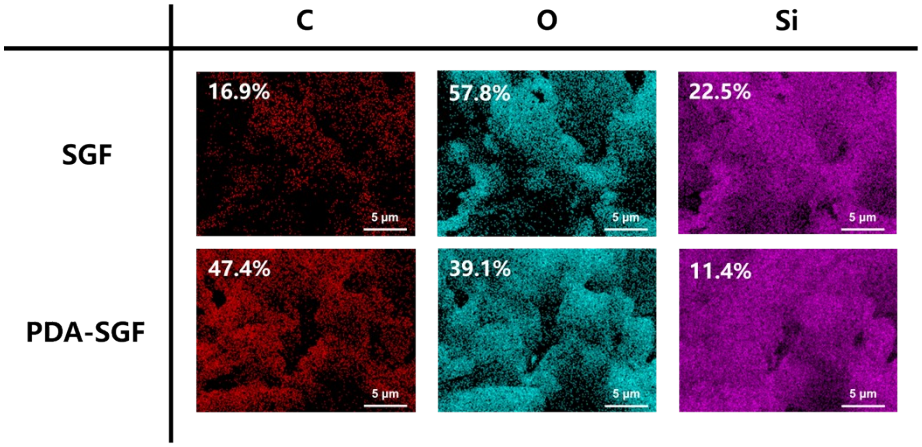

Fig. S3 Surface element distribution and proportion of SGF and PDA-SGF, measured via EDX.

4. Wide XPS Spectra of the Substrate SGF and PDA-SGF.

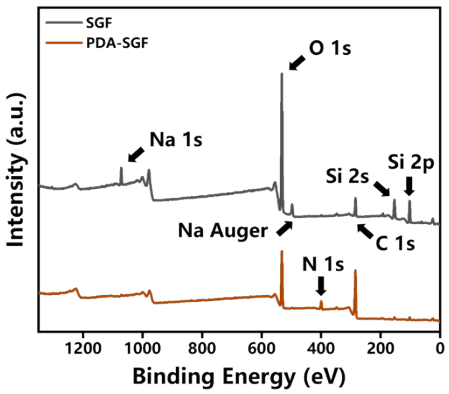

Fig. S4 Wide XPS spectra of the substrate SGF and PDA-SGF.

5. Stability of Oil-in-Water (O/W) and Water-in-Oil (W/O) Emulsions.

The O/W emulsions, W/O emulsions, and low-water-content crude oil used in the experiment were allowed to stand for 90 days. It was observed that all the emulsions remained unbroken after long-term standing, confirming their stability.

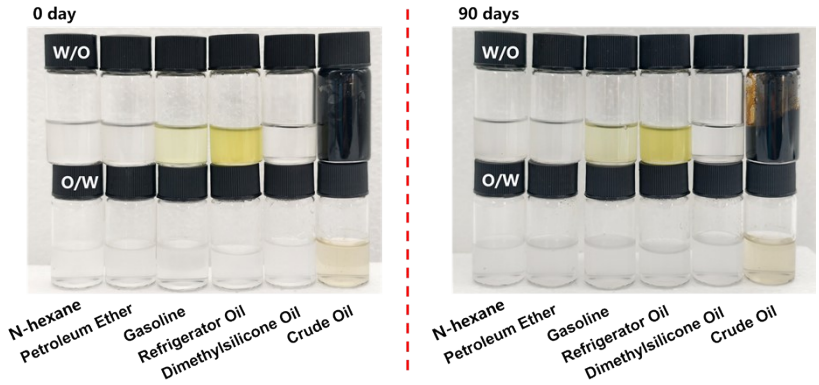

Fig. S5 Physical demonstration of O/W emulsions, W/O emulsions, and low-water-content crude oil before and after 90 days of standing.

6. Demonstration of O/W Emulsions Before and After Separation.

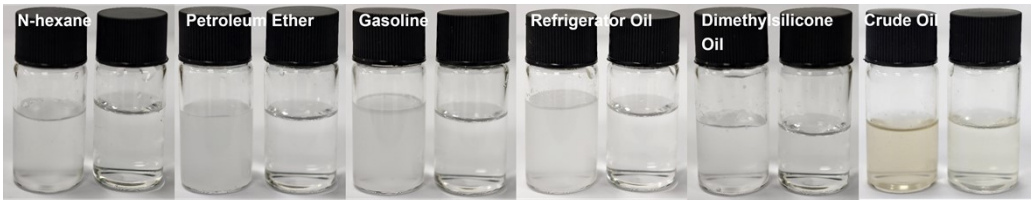

Fig. S6 Visual demonstration of O/W emulsions before and after separation.

7. Difference of W/O Emulsions and Crude Oil Before and After Separation.

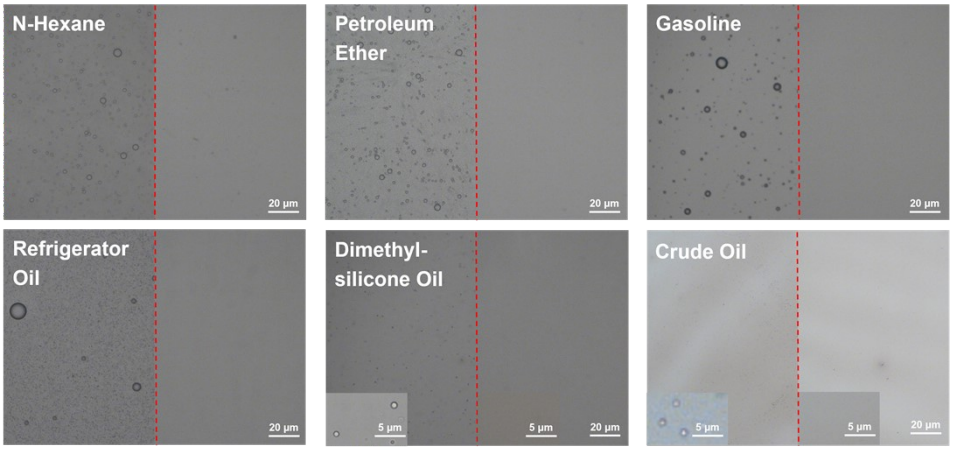

Fig. S7 Polarizing microscope images of different W/O emulsions and crude oil before and after separation.

8. Comparison of Emulsions Before and After Pressure Application.

The adding pressure device was used to continuously squeeze the emulsions at 3 bar for 30 min. After pressure application, the changes in droplets before and after pressurization were observed via polarizing microscope. Although there have been studies shown that emulsions may undergo changes under a pressure of 20 bar or higher (the droplet sizes tend to be uniform, with no large droplets present, and the droplet movement speed slows down), there was no significant difference in the dispersed phase droplets under the pressure applied in this paper, as shown in the figure below (taking dimethylsilicone oil emulsions as the example).[1] Therefore, we consider that pressurization does not exert a significant impact on the emulsion state in this study.

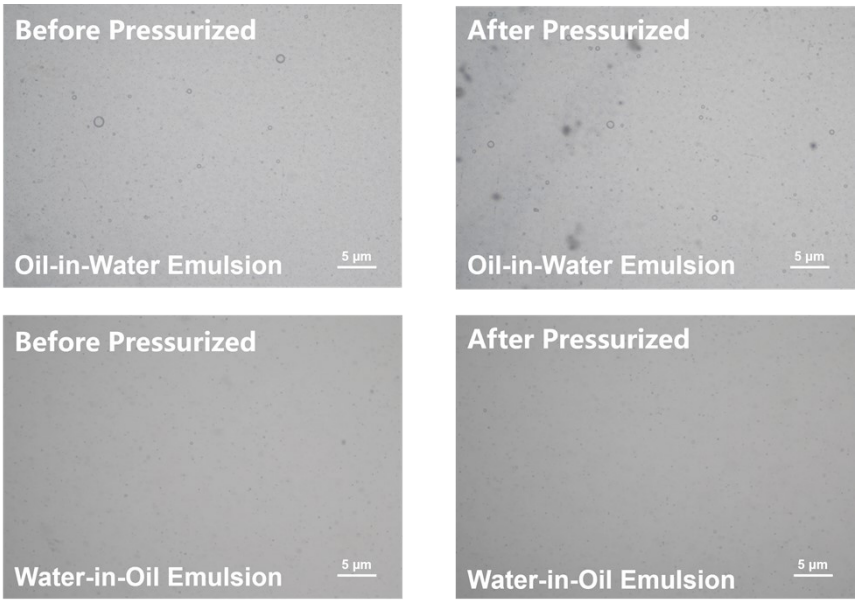

Fig. S8 Comparison the difference of dispersed phase droplets of emulsions before and after 3 bar pressure application.

9. Blocked-phase Penetration Induced by High Pressure at the End of Separation.

To verify that when the liquid seal disappears, the blocked phase is dragged into the material interior by air due to the significant pressure difference between the two surfaces of filter, we conducted filtration tests under different pressures using the separation of petroleum ether-in-wateremulsion as an example. After filtration, we observed the penetration depth of dyed droplets. As shown in the left figure, when separation was terminated before the complete removal of the upper filtrate, no penetration was observed inside the material, confirming that this phenomenon occurs at the final stage of separation. At 1 bar (the theoretical maximum pressure achievable by vacuum filtration), almost no dye traces were detected on the filter cross-section. However, with increasing pressure, the penetration depth of petroleum ether into the filter gradually increased, verifying that pressure is the primary cause of this phenomenon.

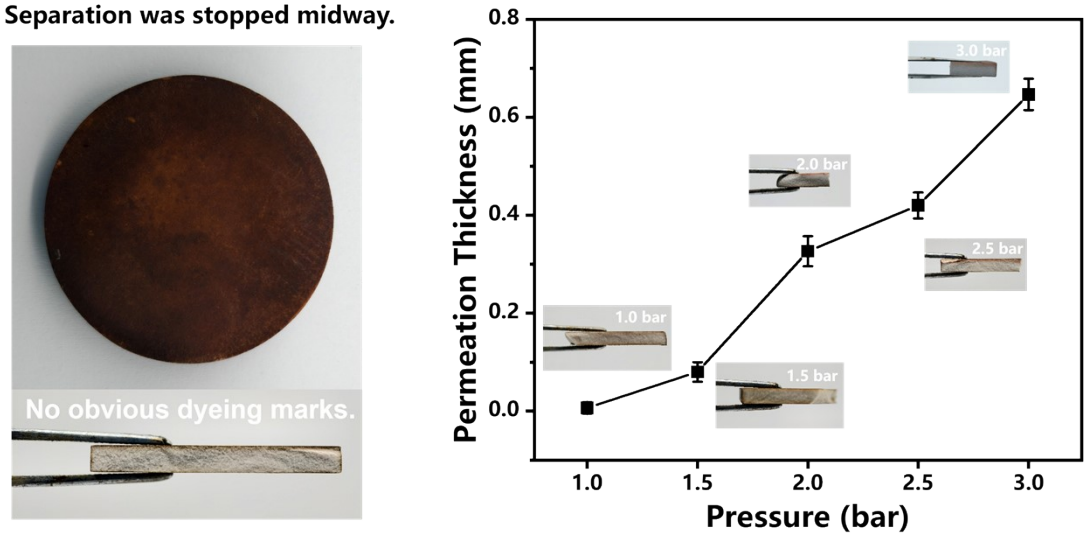

Fig. S9 The relationship between separation pressure and the penetration thickness of the blocked liquid in the filter.

10. Underwater Oil Contact Angle of Unmodified Sintered Glass Filter Substrate.

The average underwater oil contact angles of the sintered glass filter substrate toward various oils used in the experiment all exceed 150°, demonstrating that the unmodified interior of the material exhibits excellent oil-repellent capability under wet conditions. This verifies the viewpoint proposed in the manuscript that the inner layer of MPA-SGF at the separation end prevents oil from being pushed through the material.

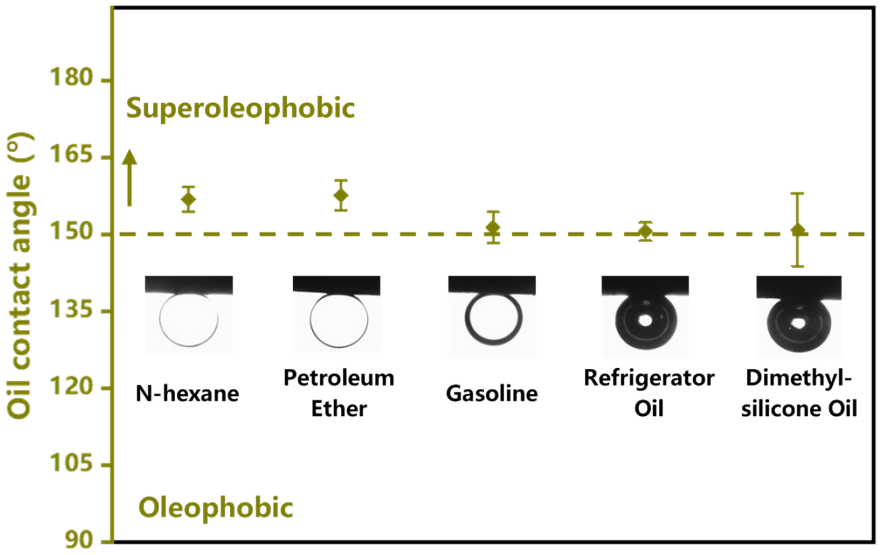

Fig. S10 Underwater oil contact angle of the unmodified sintered glass filter substrate.

Supplementary Table.

Table 1. Comparison with previously reported works of **surfactant-stabilized crude oil**-in-water emulsion separation.

S.N.	Filtration method and pressure difference borne by the material (bar)	Viscosity of crude oil used (mPa s)	Flux (L m^{-2} h^{-1})	Efficiency (%)	Reference
1	Suction filtration (0.8)	674.08	996.8	99.7	[2]
2	Suction filtration (0.75)	NA	810	99.7	[3]
3	Suction filtration (0.5)	NA	356.5	98.2	[4]
4	Suction filtration (NA)	80	2,198	99.8	[5]
5	Suction filtration (0.5)	NA	585	99.41	[6]
6	Suction filtration (0.5)	NA	2,430	99.79	[7]
7	Suction filtration (0.8)	674.08	816	99.3	[8]
8	Gravity-driven filtration	23.2	4,725	96.2	[9]
9	Cross flow filtration	NA	2,154	99	[10]
10	Cross flow filtration	NA	984.2	99.08	[11]
11	Pressure-driven filtration (3.0)	11,557	552.5	99.62	Our Previous work [12]
12	Pressure-driven filtration (3.0)	11,557	**21,139**	99.4	**This work**

* In the table, content replaced by "NA" (not available) means the relevant information is not mentioned in the article. Moreover, we have standardized the different units of flux and crude oil viscosity from the cited studies to facilitate intuitive comparison.

Table 2. Comparison with previously reported works of **surfactant-stabilized** water-in-oil emulsion **high flux** separation.

S.N.	Pressure difference borne by the material (bar)	Types of oil	Flux (L m^{-2} h^{-1})	Efficiency (%)	Reference
1	0.008	Carbon tetrachloride	4,395	＞92	[13]
2	0.00093	N-hexane	3,000	＞99.7	[14]
3	0.00625	Petroleum ether	8,140	＞99.995	[15]
4	0.4	N-decane	43,000	99.95	[16]
5	0.5	Toluene	37,526	99.95	[17]
6	**3.0**	N-hexane	**50,798**	99.8	**This work**

* In the table, we have standardized the different units of flux and pressure defference the material bore from the cited studies to facilitate intuitive comparison.

Table 3. Stability of R_m for Click-SGF under long-term high pressure separation (taking MPA-SGF for the separation of petroleum ether-in-water emulsion as an example).

Number of separation cycles	Pressure difference (bar)	Viscosity of the continuous phase (mPa s)	Flux (L m^{-2} h^{-1})	R_m (m^{-1})
1	3.0	1	18027	5.99×10^{10}
5	3.0	1	20833	5.18×10^{10}
10	3.0	1	18220	5.93×10^{10}
15	3.0	1	18404	5.87×10^{10}
20	3.0	1	20169	5.35×10^{10}
25	3.0	1	19031	5.68×10^{10}
30	3.0	1	19642	5.50×10^{10}

* The data in the table and the calculation formula are derived from Fig. 3g and equation (4) in the manuscript, respectively.

Reference:

1. M. Yang, S. Liu, L. Hou, J. Xu, *Phys. Fluids*, 2025, **37**, 043331.
2. B. Xiang, J. Gong, Y. Sun, W. Yan, R. Jin and J. Li, *J. Membr. Sci.*, 2024, **691**, 122247.
3. Q. Zhong, G. Shi, Q. Sun, P. Mu and J. Li, *J. Membr. Sci.*, 2021, **640**,119836.
4. A. A. R. Abdel-Aty, Y. S. A. Aziz, R. M. G. Ahmed, I. M. A. ElSherbiny, S. Panglisch, M. Ulbricht and A. S. G. Khalil, *Sep. Purif. Technol.*, 2020, **253**, 117467.
5. J. Meng, J. Zhang, X. Shen, J. Xie, Q. Liao, F. He, J. Zhao and Z. Wang, *Chem. Eng. J.*, 2023, **473**, 145519.
6. J. Udomsin, A. Prasannan, C.-F. Wang, J.-K. Chen, H.-C. Tsai, W.-S. Hung, C.-C. Hu and J.-Y. Lai, *J. Membr. Sci.*, 2021, **636**, 119568.
7. J. Udomsin, C.-C. Hu, C.-F. Wang, J.-K. Chen, H.-C. Tsai, S.-W. Kuo, W.-S. Hung and J.-Y. Lai, *Sep. Purif. Technol.*, 2023, **322**, 124349.
8. B. Xiang, J. Gong, Y. Sun and J. Li, *J. Hazard. Mater.*, 2024, **462**, 132803.
9. L. Xu, J. Zhang, T. Wang, Y. Cai, F. Feng, F. He and L. Yi, *Colloid Surfaces A*, 2024, **691**, 133863.
10. U. Baig, A. Waheed, J. Usman and I. H. Aljundi, *ACS Appl. Mater. Interfaces*, 2024, **16**, 33504-33516.
11. Y. Wan, L. Ma, T. Wang, G. Zhang, X. Li, J. Liao, M. Jiang and L. Zhang, *J. Membr. Sci.*, 2023, **685**, 121922.
12. W. Wang, Y. Tian, Y. Liu, W. Cao, Y. Qiu, S. Zhao, Y. Wei and L. Feng, *Sep. Purif. Technol.*, 2026, **382**, 135946.
13. H. Chen, Z. Zuo, Q. Tian, S. Xue, F. Qiu, X. Peng and T. Zhang, *J. Cleaner Prod.*, 2023, **396**, 136502.
14. H. Wu, X. Shen, M. Wei, F. Zhang, Z.-X. Low and W. Xing, *J. Membr. Sci.*, 2026, **740**, 124964.
15. Y. Si, Q. Fu, X. Wang, J. Zhu, J. Yu, G. Sun and B. Ding, *ACS nano*, 2015, **9**, 3791-3799.
16. B. Wang, A. Mahmood, L. Chen, D. Weng, C. Wang, C. Chen, Z. Li and J. Wang, *Chem Commun (Camb)*, 2020, **56**, 11585-11588.
17. X. Han, J. Hu, K. Chen, P. Wang, G. Zhang, J. Gu, C. Ding, X. Zheng and F. Cao, *Chem. Eng. J.*, 2018, **352**, 530-538.